Trace photoacoustic SO$_2$ gas sensor in SF$_6$ utilizing a 266 nm UV laser and an acousto-optic power stabilizer

BAISONG CHEN,[1] HAOKUN LI,[1] XIAOMING ZHAO,[1] MIAO GAO,[1] KUN CHENG,[1] XIAOPENG SHAO,[1] HONGPENG WU,[2,3] LEI DONG,[2] ⓘ **AND XUKUN YIN[1,4,5,*]** ⓘ

[1] *School of Optoelectronic Engineering, Xidian University, Xi'an 710071, China*
[2] *State Key Laboratory of Quantum Optics and Quantum Optics Devices, Institute of Laser Spectroscopy, Shanxi University, Taiyuan 030006, China*
[3] *State Key Laboratory of Integrated Optoelectronics, College of Electronic Science and Engineering, Jilin University, Changchun 130012, China*
[4] *State Key Laboratory of Applied Optics, Changchun Institute of Optics, Fine Mechanics and Physics, Chinese Academy of Sciences, Changchun, 130033, China*
[5] *Key Laboratory of Space Precision Measurement Technology, Xi'an Institute of Optics and Precision Mechanics Chinese Academy of Sciences, Xi'an, 710119, China*
*xkyin@xidian.edu.cn

Abstract: A sulfur dioxide (SO$_2$) gas sensor based on the photoacoustic spectroscopy technology in a sulfur hexafluoride (SF$_6$) gas matrix was demonstrated for SF$_6$ decomposition components monitoring in the power system. A passive *Q*-switching laser diode (LD) pumped all-solid-state 266 nm deep-ultraviolet laser was exploited as the laser excitation source. The photoacoustic signal amplitude is linear related to the incident optical power, whereas, a random laser power jitter is inevitable since the immature laser manufacturing technology in UV spectral region. A compact laser power stabilization system was developed for better sensor performance by adopting a photodetector, a custom-made internal closed-loop feedback controller and a Bragg acousto-optic modulator (AOM). The out-power stability of 0.04% was achieved even though the original power stability was 0.41% for ∼ 2 hours. A differential two-resonator photoacoustic cell (PAC) was designed for weak photoacoustic signal detection. The special physical constants of SF$_6$ buffer gas induced a high-*Q* factor of 85. A detection limit of 140 ppbv was obtained after the optimization, which corresponds to a normalized noise equivalent absorption coefficient of 3.2×10^{-9} cm^{-1}WHz$^{-1/2}$.

1. Introduction

Sulfur dioxide (SO$_2$) as a well-known and major atmospheric pollution gas is strictly monitored since it has a strong stimulating effect on the mucosa of eyes and respiratory tract. SO$_2$ is colorless and has a strong pungent smell. Pulmonary edema, laryngeal edema, vocal cord spasm and suffocation can be caused when dangerous amounts of SO$_2$ are breathed in. Therefore, the SO$_2$ concentration needs to be monitored in industry, such as wastewater treatment, safety production, especially when operating underground. In the electric-power industry, SO$_2$ is produced inside the sulfur hexafluoride (SF$_6$) gas-insulated substation (GIS) when decomposition mechanisms occur during corona discharges and sparks. By online monitoring of the SO$_2$ gas concentration inside the GIS in situ, the inner condition of the insulation system can be obtained without stopping working and opening the devices. The different SO$_2$ concentration level indicates the different insulation defect occurring inside the GIS. The SO$_2$ content at levels ranging from 1 to 5 parts per million by volume (ppmv), latent fault defect may be involved within the GIS. The potential fault for overheating is high when SO$_2$ concentration is > 10 ppmv. The unavoidable

impurity (H_2O vapor) in pure SF_6 will react with SO_2 to generate acidic decompositions, which may corrode the internal surface of the GIS and eventually cause a serious accident [1–4]. Numerous chemical-based detection methods have been used for the operating state diagnostic of SF_6 gas insulated equipment by detecting SO_2. In 2012 [5], a TiO_2 nanotube array sensor was reported for detecting the SF_6 decomposition product. The SO_2 concentration within 10 - 50 ppmv creates a pronounced resistance change in the nanotube array, but the poor detection sensitivity and high working temperature of 200 °C limits the sensor application. In 2021 [6], the adsorption of Sc-doped MoS_2 monolayer for SF_6 characteristic decomposition gases was reported by using a density functional theory (DFT) method. Besides, a Ru-doped MoS_2 monolayer was also investigated as a resistance-type sensor for detecting SO_2 and SOF_2 [7], the complicated sensor structure and poor long-term stability are not beneficial to practical application.

The photoacoustic spectroscopy (PAS) technique is widely investigated recently, due to its extremely high detection sensitivity and selectivity, fast response time, cost-effectiveness and compact absorption detection module [8–12]. The PAS technique is based on the target molecular absorption of the optical energy, which results in the excitation of molecular energy levels (electronic, rotational, and vibrational). The absorption lines are specific for each target molecular like a person's fingerprint. The excited state loses its energy through radiation processes, in which acoustic or ultrasonic waves are generated instantaneously due to localized transient heating and expansion. A photoacoustic transducer, usually a microphone, a quartz tuning fork (QTF), or a fiber tip, will be used to detect the pressure fluctuations [13–16]. One superiority of the PAS is the wavelength-independent relationship between the excitation wavelength and the PAS detection module. For the detection of SO_2 molecules, the strongest infrared absorption spectroscopy is between 7.2 - 7.6 μm spectral range (v_3 bands) according to the *HITRAN* database. A ppb-level detection limit was obtained in a N_2 buffer gas, which is sufficiently sensitive for decomposition monitoring in power equipment [17]. However, the SF_6 concentration in power system is typical > 99.8%. In this case, SF_6 molecules exist dense and strong absorption lines when the excitation wavelength > 6 μm despite these lines are not disclosed in the *HITRAN* database [18]. Furthermore, the expensive and hulky QCL laser (usually needs a water-cooling chiller) limits its application. For a non-interfering monitoring of SO_2 component, the ultraviolet (UV) spectral region is a superior choice, since the line strengths of electronic transitions are several orders of magnitude stronger than the ro-vibrational transitions in the near-infrared region. The UV lasers emitting at 225.7 nm and 302 nm were employed for the SO_2 detection in N_2 gas but not meeting the carrier gas requirement [19,20]. A ppbv-level SO_2 sensor in SF_6 was reported with a diode-pumped solid-state laser of 303.6 nm [21]. A UV excimer lamp as the excitation for the absorption spectroscopy was established with the light power fluctuating around 21.7 mW [22]. However, a random laser power jitter is inevitable since the immature laser manufacturing technology in UV spectral region. For the photoacoustic gas sensor, the signal amplitude S_a is related to the cell constant C, the incident optical power P_0 and the molecular absorption coefficient α, i.e., $S_a = C\alpha P_0$ [11]. The excitation laser power instability will result in an unstable photoacoustic signal for a long-term practical application.

In this manuscript, a passive Q-switching laser diode (LD) pumped all-solid-state laser emitting at ~ 266 nm was used to energetically excite SO_2 molecules. A Bragg acousto-optic modulator (AOM) together with an internal closed-loop feedback controller was adopted as a power stabilization system for a super-stable laser output power. A miniature differential photoacoustic cell (PAC) was designed for photoacoustic wave detection with a resonant frequency of 690 Hz and a high-Q factor of 85, which achieved a ppbv-level detection limit for SO_2 detection in SF_6 gas.

2. Excitation laser source

According to the MPI-Mainz database, SO_2 molecule has three absorption bands in the UV spectral region (170-400 nm). As shown in Fig. 1, A. the second allowed band of 170-240 nm ($^1B_2 \leftarrow ^1A_1$), which is the strongest, B. the first allowed band of 240-340 nm ($^1A_2$, $^1B_1 \leftarrow ^1A_1$), and C. a weak forbidden band of 340-400 nm ($^3B_1 \leftarrow ^1A_1$), which is the weakest. However, another dominating SF_6 decomposition gas (H_2S) exhibits strong electronic absorption between 160 nm-250 nm. The absorption cross interference of different decomposition components results in a gas signal overlapping, therefore the UV laser wavelength located in the spectral region B is the optimum solution [23].
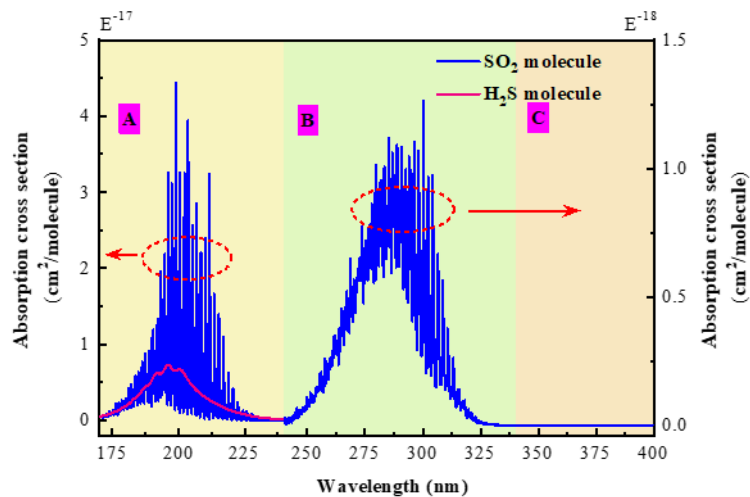

Fig. 1. Three absorption bands of H_2S and SO_2 molecules.

3. Photoacoustic sensor system

The photoacoustic signal amplitude is proportional to the excitation power of the laser excitation source. With the development of the frequency-doubling technology, the 266 nm laser output power can be reaching several hundreds of mW even watt level [24]. The stability of the power affects the detection accuracy of the sensing system. However, the output power of commercial UV lasers will fluctuate due to these factors such as operating temperature, mechanical vibration, electromagnetic interference, discharge current, and activation medium gain coefficient.

A frequency conversion of Q-switched laser emitting at 266.4 nm (Changchun new industries, model MOL-F-266) with a max average output power of 30 mW was employed as the excitation source. The pulse repetition rate of the laser current was set as the PAC resonant frequency. The transverse mode of the laser beam is near TEM_{00}, which has a beam quality factor (M^2) of < 2. The elliptical beam (4:1) diameter is < 1.2 mm with a full divergence angle of < 1.5 mrad. The average power stability over 4 hours is < 5%, which is a significant disincentive to acoustic signal detection for long-time monitoring. As shown in Fig. 2(a), a closed-loop feedback power stabilization system was designed for a super-stable photoacoustic SO_2 detection in SF_6 buffer gas. The UV laser beam passes through an AOM in the Bragg diffraction configuration with the linear polarization. The AOM can be operated in 240-400 nm, which has a diffraction efficiency of >90%. The AOM driver is commercially available (China Electronics Technology Group Corporation 26 Research Institute), which has a rise and fall time of < 10 ns. The output light was divided into the first-order beam (which was blocked further away) and the zero-order beam.

For this experiment, only the zero-order beam is the useful beam, the transmitted beam ($\sim 95\%$ power ratio) was employed to detect SO_2 gas by a differential photoacoustic cell (as shown in Fig. 2 (b)), and the reflected beam ($\sim 5\%$) was collected by a silicon avalanche photodiode (Thorlabs, APD440) to act as the feedback control beam. The photodiode voltage signal was converted into a 24-bit digital signal by a custom-made A/D converter (ADS1255). The sample frequency was set as 30 kHz. A power deviation value can be obtained by the actual photodiode digital signal and the setting power digital signal, which was employed to obtain a real-time AOM control voltage signal by utilizing a Field Programmable Gate Array (FPGA) with an incremental PID control algorithm. The AOM control voltage signal was then transmitted to an electrical controller to carry out the servo controls of the power balance between AOM diffraction orders. The zero-order power fluctuation can be alleviated by compensating for the first-order beam power. The laser output power fluctuation was transferred to the first-order power variation by the Bragg diffraction, and the goal of stabilizing the zero-order laser output power of the system was achieved. The used digit circuit exists a distinct advantage over the analog circuit published before [25–28], because it is easy to adjust equipment by editing program. Analog circuit processing analog volume is completed through the circuit structure, to solve the interference, distortion and other problems, the structure is complex and debugging is difficult. Particularly when optical wavelength of the excitation laser source changes, the feedback resistance of the analog circuit should be optimized. The actual photo and the 3D schematic diagram of the developed feedback laser power controller were shown in Fig. 2(c) and (d).
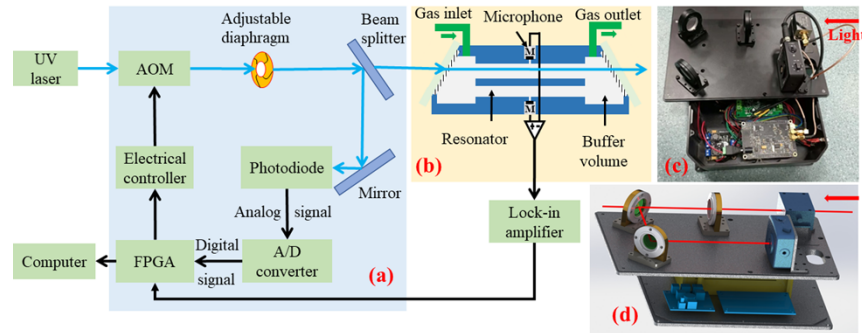

Fig. 2. Schematic diagram of photoacoustic SO_2 gas detection system with a closed-loop feedback power controller (a), a differential photoacoustic cell (b) and a lock-in amplifier. (c) and (d) are the actual photo and 3D mode of the laser power stabilization system.

The stable zero-order laser beam passed through a Helmholtz two-channel differential PAC to detect the desired SO_2 photoacoustic signal. The length and diameter of each resonator were 11 cm and 0.8 cm. Two buffer volumes with a Brewster angle were used on either side of the resonator to minimize laser beam multiple reflections and to reduce gas flow noise. Two electret condenser microphones were selected to achieve an identical signal response of around 1 kHz and mounted on the middle of each resonator. A custom-made differential pre-amplifier was used to collect the microphone current signals with a gain factor of 13. The voltage signal was fed into a lock-in amplifier (FEMTO, LIA-BVD-150) in the $1f$ mode. The decomposition photoacoustic signal was collected by the FPGA and then transferred to a computer. The filter slope of the lock-in amplifier was set as 12 dB/oct. The time constant was 1 s, which corresponded to a detection bandwidth of 0.25 Hz.

4. Laser power stability assessment

In order to verify the effect of the system control on the laser power fluctuation, the system output power needs to be quantitatively analyzed. Another silicon avalanche photodiode detector was used to detect the transmitted light beam power. The detector voltage was recorded by a six and a half digit multimeter (Agilent, 34410 A). The acquisition time interval was 1.2 s. Since the direct output data of the detector was voltage value, the voltage value is used to analyze the fluctuation of the laser output power in the following experiments. An evaluation coefficient S was used to evaluate the power stability:

$$S = \sqrt{\sum_{k=1}^{n} (P_k - \bar{P})^2 / n} / \bar{P} \tag{1}$$

in which $\bar{P} = \sum_{k=1}^{n} P_k / n$, P_k was the transmitted output laser power value obtained by sampling time k, n was the total sampling number.

The stability performance of the photodiode detector was first tested for long-term work. The light-sensitive surface of the detector was covered with a black light shield. And the enlargement factor was set as 30 dB. The voltage of the used photodiode detector was continually recorded for about two hours. As shown in Fig. 3(a), a maximal voltage changing value was < 30 µV, which means that the system accuracy was not affected by the detector dark current. Afterward, the photodiode voltage was sampled for 5,000 points in a row before and after starting the 266 nm laser power stabilization system. The comparative data were depicted in Fig. 3(b). A fluctuation coefficient S_1 of 0.41% was obtained using Eq. 1 for the UV laser power. The maximum voltage fluctuation was 38.3 mV. Commendably, a stabilized coefficient S_2 of 0.04% was achieved after starting the power stability control system. In this case, the maximum voltage fluctuation was 8.1 mV. The laser power fluctuation was significantly suppressed, and the degree of power instability was down by an order of magnitude.
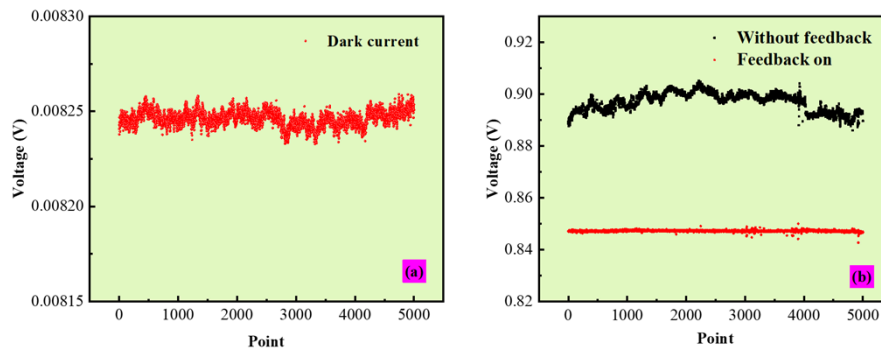

Fig. 3. (a) Photodiode voltage of the detector dark current. (b) The original (without feedback) and stable laser output power voltage.

5. Sensor performance assessment

For the sensor performance evaluation, 50 ppmv SO_2/SF_6 gas mixtures and pure SF_6 gas were used to prepare different desired SO_2/SF_6 gas concentrations by utilizing a gas dilution system (Environics Inc., EN 4000). The sensor gas flow and pressure were maintained with a diaphragm pump and a pressure controller (MKS Instruments, 649B). The experimental environment was controlled at room temperature and under standard atmospheric pressure. To obtain an optimal photoacoustic signal, the PAC resonant frequency was measured first, which was proportional to the ratio of the sound velocity υ and the resonator length L ($f = \upsilon/2L$). A PAC fundamental longitudinal vibration frequency of 690.4 Hz was obtained with a high Q-factor of 85. The

detailed description of the SF_6 buffer gas-induced high Q-factor (> 50) PAC was demonstrated previously [11], since its particular physical property relative to N_2. Therefore, the modulation frequency of the laser current was set as the PAC vibration frequency of 690.4 Hz. The duty cycle of the modulation square signal was 50%.

As shown in Fig. 4, continuous photoacoustic signal values were recorded under different concentrations of SO_2/SF_6 gas mixtures from 5 ppmv to 20 ppmv for 100 s (1 point per 1 s). The standard deviations (1σ) of pure SF_6 gas signals were defined as the sensor noise levels, which was 1.8 μV. For the sensor detection limit analysis, the average signal amplitude of 64.34 μV of 5 ppmv SO_2/SF_6 gas mixture was used. A signal-to-noise ratio (SNR) of 35.7 was obtained, which resulted in a detection limit of 140 ppbv and a normalized noise equivalent absorption (NNEA) coefficient of $3.2 \times 10^{-9} \, \text{cm}^{-1}\text{WHz}^{-1/2}$ by taking into account the laser power and the lock-in detection bandwidth.
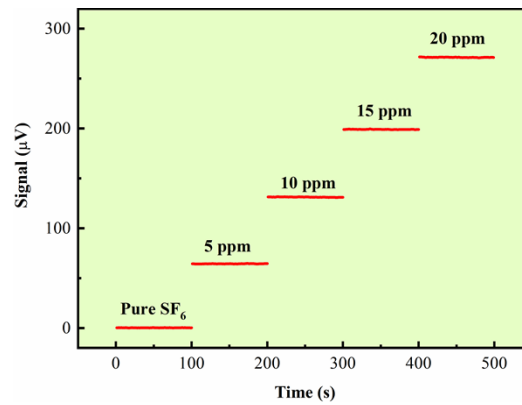

Fig. 4. Photoacoustic signal amplitudes as a function of five different SO_2/SF_6 gas mixtures.

To verify the developed sensor linear concentration response, the 50 ppmv SO_2/SF_6 gas mixtures were diluted with pure SF_6 to generate different concentration levels. The measured average photoacoustic signal amplitudes for 100 points were plotted in Fig. 5 as a function of the SO_2 concentrations. A calculated R-square value of 0.9997 was calculated for a linear fitting
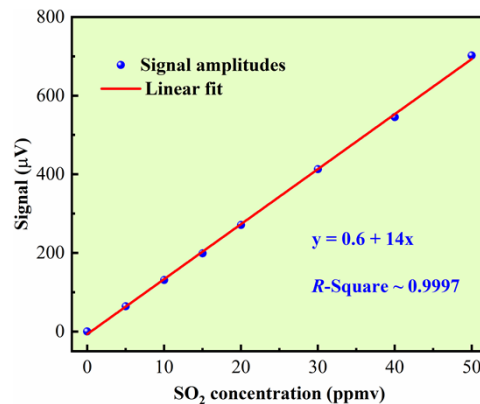

Fig. 5. Response linearity of SO_2 photoacoustic signal amplitudes for different SO_2/SF_6 gas mixtures.

analysis, which indicated that the sensor system exhibited a super linear response under different target gas molecules after adopting a power stabilization system.

6.   Conclusions

A ppb-level photoacoustic SO_2 gas sensor in a SF_6 buffer gas was demonstrated by employing a dual-resonator differential photoacoustic cell. A super-stable laser output power at 266 nm was developed using a Bragg acousto-optic modulator (AOM) together with an internal closed-loop feedback controller. A power stabilization factor of ~ 10 times was achieved with respect to the raw laser power. Such stable laser power was vital for practical application in the long operation. In addition, one of the advantages of the photoacoustic gas sensor is the wavelength-independent relationship between the PAS spectrophone and excitation light source. The power stabilization system can also be used for the different excitation light at another wavelength by adjusting the wavelength dependent devices, such as the AOM, reflector and photoelectric detector. Furthermore, the AOM can provide a power modulation function for a laser source without the modulation capability instead of using an external chopper [29]. The sensor performance with a detection limit of 140 ppbv (< 1 ppmv) and an NNEA coefficient of $3.2 \times 10^{-9}\,cm^{-1}WHz^{-1/2}$ were obtained, which was sensitive enough for the safety monitoring in the electrical power system.

Disclosures. The authors declare no conflicts of interest.

Data availability. Data underlying the results presented in this paper are not publicly available at this time but may be obtained from the authors upon reasonable request.

References

1. F. Y. Chu, "SF_6 decomposition in gas-insulated equipment," IEEE Trans. Elect. Insul. **EI-21**(5), 693–725 (1986).
2. V. Spagnolo, P. Patimisco, S. Borri, G. Scamarcio, B. E. Bernacki, and J. Kriesel, "Part-per-trillion level SF_6 detection using a quartz enhanced photoacoustic spectroscopy-based sensor with single-mode fiber-coupled quantum cascade laser excitation," Opt. Lett. **37**(21), 4461–4463 (2012).
3. X. Yin, H. Wu, L. Dong, W. Ma, L. Zhang, W. Yin, L. Xiao, S. Jia, and F. Tittel, "Ppb-level photoacoustic sensor system for saturation-free CO detection of SF_6 decomposition by use of a 10 W fiber-amplified near-infrared diode laser," Sensors and Actuators B: Chemical **282**, 567–573 (2019).
4. P. Wang, W. Chen, J. Wang, J. Tang, Y. Shi, and F. Wan, "Multigas analysis by cavity-enhanced Raman spectroscopy for power transformer diagnosis," Anal. Chem. **92**(8), 5969–5977 (2020).
5. X. Zhang, J. Zhang, Y. Jia, P. Xiao, and J. Tang, "TiO2 nanotube array sensor for detecting the SF6 decomposition product SO2," Sensors **12**(3), 3302–3313 (2012).
6. B. Li, Q. Zhou, R. Peng, Y. Liao, and W. Zeng, "Adsorption of SF_6 decomposition gases (H_2S, SO_2, SOF_2 and SO_2F_2) on Sc-doped MoS_2 surface: A DFT study," Appl. Surf. Sci. **549**, 149271 (2021).
7. G. Zhang, Z. Wang, and X. Zhang, "Theoretical screening into Ru-doped MoS_2 monolayer as a promising gas sensor upon SO_2 and SOF_2 in SF_6 insulation devices," Mol. Phys. E2018517 (2021).
8. P. Patimisco, A. Sampaolo, L. Dong, F. Tittel, and V. Spagnolo, "Recent advances in quartz enhanced photoacoustic sensing," Appl. Phys. Rev. **5**(1), 011106 (2018).
9. H. Wu, L. Dong, H. Zheng, Y. Yu, W. Ma, L. Zhang, W. Yin, L. Xiao, S. Jia, and F. Tittel, "Beat frequency quartz-enhanced photoacoustic spectroscopy for fast and calibration-free continuous trace-gas monitoring," Nat. Commun. **8**(1), 15331 (2017).
10. T. Wei, A. Zifarelli, S. D. Russo, H. Wu, G. Menduni, P. Patimisco, A. Sampaolo, V. Spagnolo, and L. Dong, "High and flat spectral responsivity of quartz tuning fork used as infrared photodetector in tunable diode laser spectroscopy," Appl. Phys. Rev. **8**(4), 041409 (2021).
11. X. Yin, L. Dong, H. Wu, W. Ma, L. Zhang, W. Yin, L. Xiao, S. Jia, and F. Tittel, "Ppb-level H_2S detection for SF_6 decomposition based on a fiber-amplified telecommunication diode laser and a background-gas-induced high-Q photoacoustic cell," Appl. Phys. Lett. **111**(3), 031109 (2017).
12. Y. Hu, S. Qiao, Y. He, Z. Lang, and Y. Ma, "Quartz-enhanced photoacoustic-photothermal spectroscopy for trace gas sensing," Opt. Express **29**(4), 5121–5127 (2021).

13. Y. Ma, Y. He, L. Zhang, X. Yu, J. Zhang, R. Sun, and F. Tittel, "Ultra-high sensitive acetylene detection using quartz-enhanced photoacoustic spectroscopy with a fiber amplified diode laser and a 30.72 kHz quartz tuning fork," Appl. Phys. Lett. **110**(3), 031107 (2017).

14. K. Liu, J. Mei, W. Zhang, W. Chen, and X. Gao, "Multi-resonator photoacoustic spectroscopy," Sens. Actuators, B **251**, 632–636 (2017).

15. H. Lv, H. Zheng, Y. Liu, Z. Yang, Q. Wu, H. Lin, B. Montano, W. Zhu, J. Yu, R. Kan, Z. Chen, and F. Tittel, "Radial-cavity quartz-enhanced photoacoustic spectroscopy," Opt. Lett. **46**(16), 3917–3920 (2021).

16. Y. Cao, Q. Liu, R. Wang, K. Liu, W. Chen, G. Wang, and X. Gao, "Development of a 443 nm diode laser-based differential photoacoustic spectrometer for simultaneous measurements of aerosol absorption and NO_2," Photoacoustics **21**, 100229 (2021).

17. X. Yin, H. Wu, L. Dong, B. Li, W. Ma, L. Zhang, W. Yin, L. Xiao, S. Jia, and F. Tittel, "ppb-level SO_2 photoacoustic sensors with a suppressed absorption−desorption effect by using a 7.41 μm external-cavity quantum cascade laser," ACS Sens. **5**(2), 549–556 (2020).

18. X. Yin, L. Dong, H. Wu, L. Zhang, W. Ma, W. Yin, L. Xiao, S. Jia, and F. Tittel, "Highly sensitive photoacoustic multicomponent gas sensor for SF_6 decomposition online monitoring," Opt. Express **27**(4), A224–A234 (2019).

19. M. A. Gondal and J. Mastromarino, "Pulsed laser photoacoustic detection of SO_2 near 225.7 nm," Appl. Opt. **40**(12), 2010–2016 (2001).

20. G. Somesfalean, Z. Zhang, M. Sjöholm, and S. Svanberg, "All-diode-laser ultraviolet absorption spectroscopy for sulfur dioxide detection," Appl. Phys. B **80**(8), 1021–1025 (2005).

21. X. Yin, L. Dong, H. Wu, H. Zheng, W. Ma, L. Zhang, W. Yin, L. Xiao, S. Jia, and F. Tittel, "Highly sensitive SO_2 photoacoustic sensor for SF_6 decomposition detection using a compact mW-level diode-pumped solid-state laser emitting at 303 nm," Opt. Express **25**(26), 32581–32590 (2017).

22. T. Chen, K. Li, F. Ma, X. Qiu, Z. Qiu, Z. Liao, and G. Zhang, "Application of Excimer Lamp in Quantitative Detection of SF6 Decomposition Component SO2," Sensors **21**(24), 8165 (2021).

23. Y. Zhang, Y. Wang, Y. Liu, X. Dong, H. Xia, Z. Zhang, and J. li, "Optical H_2S and SO_2 sensor based on chemical conversion and partition differential optical absorption spectroscopy," Spectrochim. Acta, Part A **210**, 120–125 (2019).

24. Q. Liu, X. Yan, M. Gong, H. Liu, G. Zhang, and N. Ye, "High-power 266 nm ultraviolet generation in yttrium aluminum borate," Opt. Lett. **36**(14), 2653–2655 (2011).

25. V. I. Balakshy, Y. I. Kuznetsov, S. N. Mantsevich, and N. V. Polikarpova, "Dynamic processes in an acousto-optic laser beam intensity stabilization system," Opt. Laser Techno. **62**, 89–94 (2014).

26. C. D. Tran and R. J. Furlan, "Amplitude stabilization of a multiwavelength laser beam by an acoustooptic tunable filter," Rev. Sci. Instrum. **65**(2), 309–314 (1994).

27. F. Tricot, D. H. Phung, M. Lours, S. Guérandel, and E. de Clercq, "Power stabilization of a diode laser with an acousto-optic modulator," Rev. Sci. Instrum. **89**(11), 113112 (2018).

28. D. Kim, H. Rhee, J. Song, and Y. Lee, "Laser output power stabilization for direct laser writing system by using an acousto-optic modulator," Rev. Sci. Instrum. **78**(10), 103110 (2007).

29. Q. Zhang, J. Chang, Q. Wang, Z. Wang, F. Wang, and Z. Qin, "Acousto-Optic Q-Switched Fiber Laser-Based Intra-Cavity Photoacoustic Spectroscopy for Trace Gas Detection," *Sensors* 18(42), (2018).